Multiresponsive polymeric microstructures with encoded predetermined and self-regulated deformability

Yuxing Yao[a], James T. Waters[b], Anna V. Shneidman[c], Jiaxi Cui[c], Xiaoguang Wang[c], Nikolaj K. Mandsberg[c,d], Shucong Li[a], Anna C. Balazs[b], and Joanna Aizenberg[a,c,e,1]

[a]Department of Chemistry and Chemical Biology, Harvard University, Cambridge, MA 02138; [b]Chemical Engineering Department, University of Pittsburgh, Pittsburgh, PA 15261; [c]John A. Paulson School of Engineering and Applied Sciences, Harvard University, Cambridge, MA 02138; [d]Department of Micro- and Nanotechnology, Technical University of Denmark, 2800 Kongens Lyngby, Denmark; and [e]Wyss Institute for Biologically Inspired Engineering, Harvard University, Cambridge, MA 02138

Edited by Nicholas L. Abbott, University of Wisconsin–Madison, Madison, WI, and accepted by Editorial Board Member Peter J. Rossky November 6, 2018 (received for review July 9, 2018)

Dynamic functions of biological organisms often rely on arrays of actively deformable microstructures undergoing a nearly unlimited repertoire of predetermined and self-regulated reconfigurations and motions, most of which are difficult or not yet possible to achieve in synthetic systems. Here, we introduce stimuli-responsive microstructures based on liquid-crystalline elastomers (LCEs) that display a broad range of hierarchical, even mechanically unfavored deformation behaviors. By polymerizing molded prepolymer in patterned magnetic fields, we encode any desired uniform mesogen orientation into the resulting LCE microstructures, which is then read out upon heating above the nematic–isotropic transition temperature ($T_{N–I}$) as a specific prescribed deformation, such as twisting, in- and out-of-plane tilting, stretching, or contraction. By further introducing light-responsive moieties, we demonstrate unique multifunctionality of the LCEs capable of three actuation modes: self-regulated bending toward the light source at $T < T_{N–I}$, magnetic-field–encoded predetermined deformation at $T > T_{N–I}$, and direction-dependent self-regulated motion toward the light at $T > T_{N–I}$. We develop approaches to create patterned arrays of microstructures with encoded multiple area-specific deformation modes and show their functions in responsive release of cargo, image concealment, and light-controlled reflectivity. We foresee that this platform can be widely applied in switchable adhesion, information encryption, autonomous antennae, energy harvesting, soft robotics, and smart buildings.

liquid-crystal elastomers | actuators | autonomous materials multifunctionality

Arrays of dynamic, reconfigurable microstructures on biological surfaces allow living systems to alter their functional properties such as structural color (1), wettability (2), and adhesion (3, 4) in response to external stimuli. By coupling their intrinsically encrypted chemical and mechanical properties to externally applied fields, these versatile biological structures are able to exhibit area-specific motions, following not only predetermined deformations [e.g., seed release by pinecones (5)], but also self-regulated, stimuli-specific cooperative movements [e.g., setae on geckos' feet (3, 4)]. To mimic such adaptive functions found in nature, a variety of microstructural systems involving hydrogels combined with embedded microfibrils (5–7), inorganic nanoparticles (8) and nanosheets (9), and surface-attached micropillars and microplates (10) have been developed (5–12). These designs, however, rely on passive actuation mechanisms (10, 11) where the system's reconfiguration is fully determined by the actuating gel "muscle" and the stiffness and anisotropy of the embedded structures, which significantly limits the range of allowed deformations. For example, gel-embedded plate-like structures will experience only out-of-plane bending, while mechanically unfavored shape changes, such as in-plane tilting and shearing, or even some elementary deformations, such as unidirectional microstructure contraction and twisting, are hard to achieve. Moreover, unlike their natural counterparts, control over the deformation behaviors within different regions and realizing self-regulated directional motion within a synthetic microstructure array remain challenging.

Liquid-crystalline elastomers (LCEs), a class of lightly cross-linked anisotropic polymer networks (13–15), exhibit significant deformability in response to heat (16–25), light (26–31), and humidity (32), thus offering distinct advantages for designing dynamic patterned surfaces (24, 33, 34), microactuators (16–30), and soft robots (31). The reversible, macroscopic shape-changing behavior of LCEs is determined by the microscopic reconfiguration of the internal LC order, which switches between the nematic phase with aligned LC mesogens and the isotropic phase with randomly oriented mesogens. Compared with the passive actuation of structures driven by a gel muscle, LCE materials are themselves active, with the mechanical deformation and shape-changing behavior being controlled by their own chemical and material properties (16–35). However, two limitations of the current research should be mentioned. On the one hand, while in LCE thin films, which constitute the majority of studies, mesogen alignment (so-called director) can be finely tuned in 3D through chemical templating by patterned surfaces, the simple 2D

Significance

The range of allowed deformation modes currently described for the actuation of microstructures is limited. In this work we introduce magnetic-field–guided encoding of highly controlled molecular anisotropy into 3D liquid-crystalline elastomer microstructures capable of displaying unique multiresponsive, shape-changing behaviors. The richness of the predetermined and self-regulated deformations and region-specific motions in these microstructural arrays gives rise to physicochemical insights, as well as potential applications in controlled adhesion, information encryption, soft robotics, and self-regulated light–material interactions.

Author contributions: Y.Y., A.C.B., and J.A. designed research; Y.Y. and A.V.S. performed research; J.T.W., J.C., and S.L. contributed new reagents/analytic tools; Y.Y., J.T.W., A.V.S., X.W., N.K.M., and J.A. analyzed data; and Y.Y., A.V.S., and J.A. wrote the paper.

The authors declare no conflict of interest.

This article is a PNAS Direct Submission. N.L.A. is a guest editor invited by the Editorial Board.

[1]To whom correspondence should be addressed. Email: jaiz@seas.harvard.edu.

This article contains supporting information online at www.pnas.org/lookup/suppl/doi:10.1073/pnas.1811823115/-/DCSupplemental.

Published online December 4, 2018.

geometry of the films limits the range of possible deformations and thus applications (23, 24, 26–30, 32). On the other hand, although previous work has demonstrated thermal-responsive (17–22) and light-responsive (31) uniaxial contraction as well as light-responsive bending (35) of 3D LCE microstructures formed by stretching or drawing, these deformations are predominantly guided by the mechanically induced single-director orientation and lack the potential for the variety of responses that the same structures would display given an arbitrary mesogen alignment in 3D. More complex 3D microstructured LCEs beyond 1D micropillars, filaments, or 2D thin films, especially those displaying atypical actuation types (i.e., in-plane tilting and twisting), or hierarchical assembly of arrays of LCE microstructures exhibiting both predetermined and self-regulated cooperative motions have not yet been achieved.

In this article, we demonstrate a general approach for the synthesis of 3D LCE structures and their assemblies capable of a range of such hierarchical deformation behaviors, which are difficult to induce either in conventional passive actuation systems (e.g., gel-embedded structures) or in 1D and 2D LCE materials. The key to our method is applying a magnetic field (36) to program an arbitrary, magnetic-field–defined uniaxial orientation of the LC director within microstructures of any simple or complex 3D shape, followed by photopolymerization to preserve the molecular configuration (17–20). We further use complex 3D-patterned magnetic fields to create arrays of microstructures with area-specific molecular orientations, which then display either variable, locally predetermined deformations or self-regulated, dynamically changing bending motions to follow a light source when combined with light-responsive moieties. Moreover, multifunctionality and multiresponsiveness, with the ability to display different actuation modes upon exposure to different stimuli, can be achieved. We also demonstrate how such cooperative motions of LCE microstructures are useful for information encryption, controlled adhesive systems, and unique self-regulated antenna arrays. We envision that our approach can also be complementary to other material-processing methods, for example, 3D printing, to enable many more interesting deformation behaviors at the microscale and thus realize novel microactuators and their applications in various fields.

Designing LCE Microstructures with Various Predetermined Deformations

We synthesized a side-on LCE (Fig. 1*A*) using a published procedure (16) and characterized the resulting structures with NMR (*SI Appendix*, Fig. S1), differential scanning calorimetry (DSC), and polarized optical microscopy (POM) that showed the nematic–isotropic (N–I) phase transition of the LCE to occur at 125 °C (*SI Appendix*, Fig. S2). When 3D printed or pulled into a micropillar during polymerization and heated above its $T_{N–I}$, the structure experienced only one type of deformation, i.e., uniaxial contraction (25) due to a single achievable mesogen orientation along the structure upon stretching (Fig. 1*B*). However, if the director in the LCE is designed to adopt various orientations within the microstructures, the same 3D LCE shapes are expected to undergo a range of deformations. A computational model was developed to represent the LCE in a finite-element framework (37, 38) (*SI Appendix*, Fig. S3) and to illustrate the anticipated actuation types for differently oriented mesogens in an exemplary 3D shape—a rectangular microplate (Fig. 1 *C*, *i*). We employed hexahedral [initially cubic (39)] as opposed to tetrahedral elements, to easily capture the shape of the plates. The Gent model (40, 41) was used to account for the finite extensibility of the polymer chains, in contrast to the models used previously (37, 38). The computer simulations suggest that in addition to plate contraction arising from the *z*-axis director orientation (Fig. 1 *C*, *ii*), the same plate can experience elongation for the *y*-axis director orientation (Fig. 1 *C*, *iii*), out-of-plane tilting

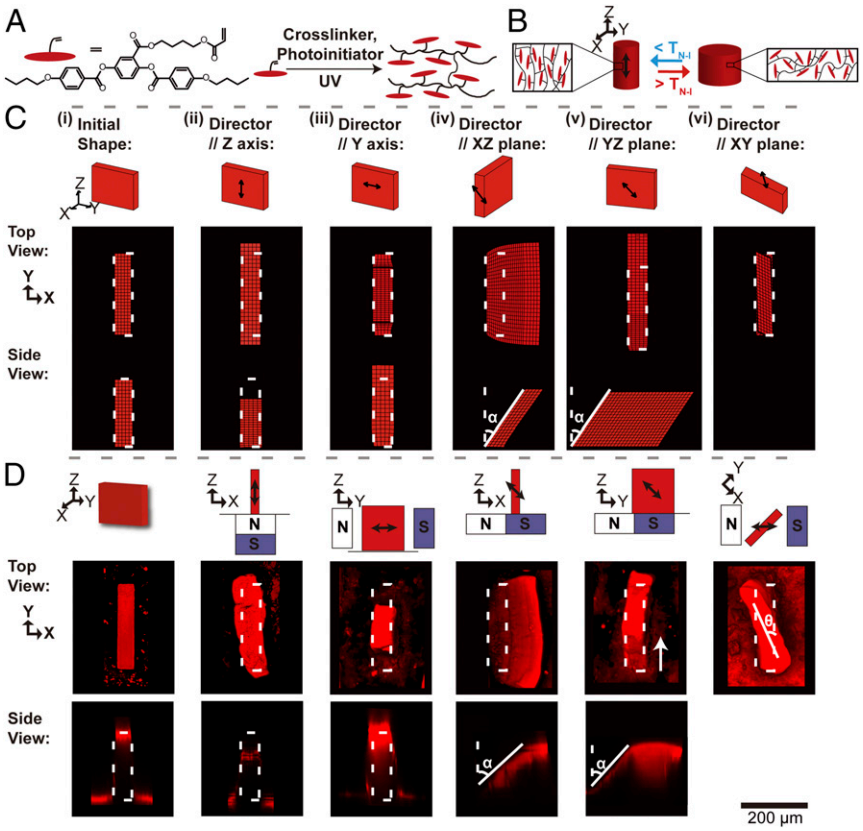

Fig. 1. Thermal-responsive LCE microplates with different internal molecular configurations. (*A*) Molecular structure of reactive LC monomer 4″-acryloyloxybutyl 2,5-di(4′-butyloxybenzoyloxy) benzoate and the polymerization process to form a side-on LCE. (*B*) Schematic illustration of the LCE micropillar that undergoes contraction during the N–I transition when the director is oriented along the structure—the case corresponding to 3D-printed or stretched microstructures. (*C*) Finite-element simulation results, showing the initial shape (*i*) and the types of deformation that will originate from the director orientation along the *z* axis (*ii*), along the *y* axis (note the contraction of the top surface in the *y* direction; *iii*), in the *x*–*z* plane (*iv*), in the *y*–*z* plane (*v*), and in the *x*–*y* plane (*vi*). White dashed outlines indicate the original shape of the microplate. (*D*, *Top*) Schematics showing the relative orientation and position of the plates (shown in red) in designed, 3D magnetic fields that give rise to the director orientations computed in *C*, *ii*–*vi*, respectively. Double-headed black arrows represent the director. (*D*, *Bottom*) Fluorescence confocal micrographs of the thermal-responsive deformation of the corresponding synthesized LCE microplates. White dashed outlines indicate the original shape of the LCE microplate. In *D*, *v*, the white arrow denotes the vector from the edge of the bottom surface to that of the top surface of the microplate, which has been shifted in the *y* direction. (*C* and *D*) The axes indicate the different planes of projection. α represents the tilting angle and θ illustrates the twisting angle.

for the director in the *x*–*z* plane (Fig. 1 *C*, *iv*), in-plane tilting for the director in the *y*–*z* plane (Fig. 1 *C*, *v*), or rectangular-to-parallelogram cross-section transformation with a slight twisting for the director orientation in the *x*–*y* plane (Fig. 1 *C*, *vi*).

To experimentally realize such a rich deformation palette, we molded the prepolymer mixture into a desired 3D shape (*SI Appendix*, Fig. S4 and Table S1) and oriented the mesogens using a magnetic field before and throughout the polymerization process (*SI Appendix*, Fig. S5). Fig. 1*D* and Movie S1 show the results for an exemplary 250-μm × 50-μm × 200-μm plate heated to above 125 °C, exhibiting a range of deformations in excellent correspondence to simulations. The plate actuation was characterized by fluorescence confocal microscopy (see *SI Appendix* for details). When heated above its $T_{N–I}$, we observed 40% shrinkage and 20% expansion, parallel and perpendicular to the director, respectively. *SI Appendix*, Table S2 summarizes the dimensions of the deformed microplates with different director orientations. We also saw negligible deformation hysteresis of the microplates during temperature cycling (*SI Appendix*, Fig. S6). The effect of mesogen alignment induced by surface anchoring to the walls of the mold during polymerization (42), which is dominant in thin, 2D films, was estimated to overrule the effect of the magnetic field when 3D LCE structures have dimensions smaller than $L_{crit} \sim 5$ μm (the mesogenic alignment of LCE microplates with any dimension smaller than L_{crit} follows surface anchoring, whereas it aligns with the magnetic field for microplates larger than L_{crit}; see *SI Appendix* for details). Indeed, 25-μm × 5-μm × 20-μm plates showed negligible deformation arising from the magnetic-field–induced mesogen alignment and followed the deformation prescribed by the walls of the structures (*SI Appendix*, Fig. S7). In contrast, for the microstructures with dimensions in the range of 25–250 μm used in this study, the surface effect is insignificant, and the deformation types are primarily defined by the orientation of the molded prepolymer in the magnetic field. Moreover, the original shape of the microstructure is "memorized" (Movie S2) and the deformation of microstructures is reversible with little deterioration, as evidenced by 20 actuating cycles immediately after synthesis and 180 additional cycles 9 mo later (see *SI Appendix*, Fig. S8 for details).

Notably, the deformations obtained when the director is oriented off but not perpendicular to the *z* axis lead to the same tilting angle α (the deflection of the microplate from its original, upright orientation) both out of plane (Fig. 1 *D*, *iv*) and in plane (Fig. 1 *D*, *v*), which is remarkable from the mechanics point of view as the in-plane bending stiffness of the microplate is ∼24 times higher than that of the out-of-plane bending. For example, a director set at 45° with respect to the *z* axis in the *x*–*z* and the *y*–*z* planes causes tilting of the microplates by the same 55° angle (Fig. 1 *D*, *iv* and *v* and Fig. 2*A*). This unique behavior cannot be observed in gel-actuated plates or any other mechanically deformable structures, which are only capable of out-of-plane bending. In contrast, the equal tilting in both directions for LCE microplates is attributed to their active actuation characteristic: The conformational change of the polymer networks extends uniformly within the bulk material, avoiding the creation of stress-concentrating regions commonly encountered in passive actuation systems at the base of substrate-attached static microstructures. Moreover, both azimuthal and polar tilting angles of an LCE microplate can be continuously tuned by adjusting the LC director during polymerization (Fig. 2*B*).

We further note that the experimentally observed twisting angle (θ, the angle between the orientation of the top surface of a deformed plate and that of its undeformed orientation) of ∼18° achieved for the LC director oriented in the *x*–*y* plane but not parallel to either axis is significantly larger than the angle of 1.7° expected based on computer simulations. We attribute this feature to the contribution from the LCE base film, which is twisting together with the microstructures, thus increasing the overall macroscopic effect. Indeed, computer simulations that take into account the base contribution do show the increase in the twist angle as a function of the base thickness (*SI Appendix*, Fig. S9). Even more interestingly, the microstructures can be programmed to undergo either right-hand or left-hand twisting (Fig. 2*C*). This result demonstrates that instead of a complex synthesis involving doping with chiral molecules (43), we can simply introduce handedness by varying the in-plane director within an achiral LCE microplate.

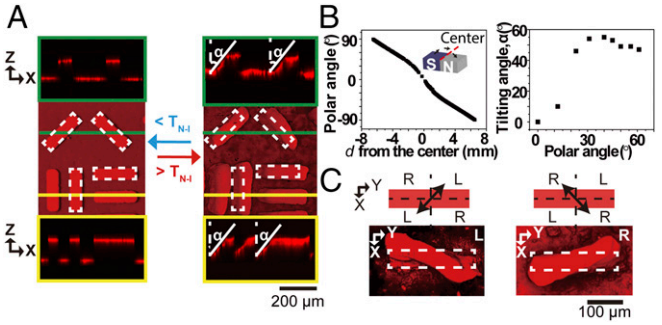

Fig. 2. Control over the deformation of 3D LCE microstructures. (*A*) Fluorescence confocal micrographs showing the tilting behavior of LCE microplates facing different directions in the magnetic field. Yellow and green panels show the reconstructed side views of the microplates at the marked regions. The tilt angle and direction are the same, irrespective of the orientation of the plates in a magnetic field. (*B*) Dependence of the tilting angle of a microplate on the polar angle of the LC director relative to the *x*–*y* plane. *B*, *Left* shows the COMSOL Multiphysics-calculated magnetic field that controls the polar angle of the LC director in the microstructures positioned at a distance *d* from the center. The continuously varying magnetic field and the associated changes in the LC director as a function of *d* result from the assembly of two block magnets with north (N) and south (S) poles pointing upward, respectively (only the top half of each magnet is shown). We define the center as the line where the magnets' N and S poles meet, shown as the red dashed line in *Inset*. Zero polar angle corresponds to the microstructures positioned at the center, where the orientation of the director is parallel to the *x*–*y* plane. *B*, *Right* illustrates the experimentally measured tilting angle α of a microplate as a function of the polar angle of the LC director. (*C*) Control over the twist handedness of microplates by tuning the in-plane LC director. (*C*, *Top*) Schematic illustration of the in-plane LC director. (*C*, *Bottom*) The corresponding fluorescence confocal micrographs of twisted microplates. When the director is rotated clockwise from the *x* axis, i.e., oriented in the region marked "L" in the schematic, the microplate adopts a left-handed twist, as shown in the corresponding micrograph (*Bottom Left*). When the director is rotated counterclockwise from the *x* axis, i.e., oriented in the region marked "R" in the schematic, the microplate adopts a right-handed twist, as shown in the corresponding micrograph (*Bottom Right*).

The above procedures can be applied to fabricate not only plates, but also any other complex 3D LCE shapes that will display completely different—largely unachievable using existing approaches—deformation types programmed by the magnetic-field–induced mesogen alignment. We demonstrate this rich actuation palette by the reconfigurations of an exemplary honeycomb microstructure that undergoes buckling, shear, or transformation into a brick-wall geometry upon the N–I transition (see Fig. 3, *SI Appendix*, and Movie S3 for details).

Controlled Patterning of Area-Specific Deformations in LCE Microstructure Arrays

Building on the above demonstrations of the programmable deformation of individual plates and the fact that more complex 3D magnetic fields can be used for mesogen orientation, we further developed two complementary methods to synthesize microstructure arrays with area-specific nonuniform actuation. First, we imposed a magnetic field with a spatial gradient during polymerization. An exemplary twofold symmetric pattern of magnets, shown in Fig. 4*A* and *SI Appendix*, Fig. S10*A*, induced spatially programmed, continuously changing mesogen

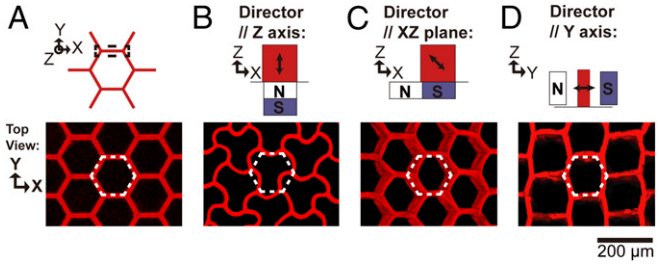

Fig. 3. Deformations of a honeycomb structure with various internal mesogenic configurations. (*A*) The schematic illustration and confocal fluorescence image of the original structure. (*B–D*) Schematics (*Top*) and confocal fluorescence micrographs (*Bottom*) showing the deformed states of the honeycomb structure with the designed mesogenic orientation. The relative position of the black dashed wall in the magnetic field is shown at *Top*. All dashed white lines indicate the structure before deformation. The black double-headed arrows represent the LC director.

orientations along the microstructure assembly, resulting in plates featuring a gradient of tilting angles from 0° to 55° upon heating to 130 °C (above $T_{N–I}$); the array forms an alternating "toward the center" and "away from the center" pattern along the *x* axis. Other types of area-specific actuations are shown in Fig. 4 *B* and *C* and *SI Appendix*, Fig. S10 *B* and *C*, where "T"-shaped and fourfold symmetric magnetic fields are used to encrypt a unique director orientation and the corresponding deformation type into every member of the array. We further illustrate one of the potential applications of such LCE microarrays in the controlled release of cargo. As demonstrated in Fig. 5*A*, when the temperature reached $T_{N–I}$, the LCE microstructures underwent predesigned downward tilting, leading to the unloading of an epoxy microstructural cargo, which remained on the LCE surface below $T_{N–I}$. These results indicate a facile way to synthesize a dynamic system mimicking the cooperativity of reversible adhesion encountered in nature.

Thus far, we have described a method to produce microstructure assemblies possessing a spatially continuous motion defined by their positioning in complex magnetic fields. We now introduce a second approach that takes advantage of the possibility to use masked, stepwise polymerization to allow for noncontinuous, area-specific deformations in the arrays of microstructures. As shown in Fig. 5*B*, the first step of polymerization was carried out under an "H"-patterned photomask in the absence of a magnetic field. Such polymerization defines an H-patterned region outside of which LCE microstructures have randomly oriented mesogens. Subsequently, we removed the photomask and conducted the second polymerization step in the presence of a magnetic field to polymerize the previously masked region inside the H. The second polymerization encodes a uniform, magnetic-field–defined mesogen orientation. As a result, while no pattern is seen in undeformed structures below $T_{N–I}$, the microstructure assembly reveals an H pattern upon the N–I phase transition due to different internal configurations and the associated deformation types preserved by the stepwise polymerization. This result suggests principles by which information can be easily encrypted into and read out by the LCE microstructures.

Multiresponsiveness and Self-Regulated Deformations of LCE Microstructures

The deformation modes discussed above were predetermined by the structure and its internal mesogen orientation controlled by the magnetic field. To expand our system further, we demonstrate that arrays of structures can also be programmed to exhibit self-regulated motion. As an example, we introduced light-responsive cross-linkers—4,4′-bis(6-acryloyloxyhexyloxy) azobenzene (Fig. 6*A* and *SI Appendix*, Fig. S11)—into the prepolymer mixture molded into an array of micropillars. The N–I transition of the resulting LCE was determined to be ∼90 °C (*SI Appendix*, Fig. S12). As illustrated in Fig. 6*B*, within the limited penetration depth of the UV light, the *trans–cis* isomerization of azobenzene groups interrupts the LC ordering, creating a bimorph that undergoes contraction of its UV-exposed side, leading to bending of the micropillars toward the light source. In Fig. 6*C*; *SI Appendix*, Fig. S13; and Movies S5 and S6, we experimentally demonstrated that the micropillars consistently follow the light when the encoded director orientation is along the *z* axis—a signature of self-regulation that is distinct from thermally activated predetermined deformations described earlier. To characterize such light-regulated motion, we coated the tips of the micropillars with silver, thereby creating a deformable micromirror array, with the micropillar tips appearing bright when directly facing the camera and dark when facing away (Fig. 6*C*, *Insets* and *SI Appendix*, Fig. S14).

We note that both predetermined and self-regulated modes can be programmed into a single microstructure to enable yet another important feature that is desired but not easily achievable in existing synthetic dynamic materials—their multifunctionality and multiresponsiveness, i.e., the ability to display different actuation modes upon exposure to different stimuli. To achieve such a behavior, we introduced light-responsive cross-linkers into the micropillar arrays, in which the director is not parallel to the *z* axis. Such micropillars can undergo three distinct deformation modes: (*i*) Thermally induced N–I transition triggers deformations predetermined by the magnetic-field–induced mesogen orientation (e.g., tilting, as shown in Fig. 6*D*, *Middle*); (*ii*) below the N–I transition, UV-induced azobenzene isomerization generates self-regulated motion that follows the light source; and (*iii*) combination of the stimuli, i.e., UV exposure at temperatures above the N–I transition, results in directional self-regulated motion with different ranges of bending angles, shown as more bending ($\beta > \alpha$) when the light is from the tilted direction of the LCE micropillar (Fig. 6*D*, *Bottom Right* and 6*E*), and backward bending ($\beta < \alpha$) when the light is from the opposite direction (Fig. 6*D*, *Top Right* and 6*E*). It is noteworthy that the latter occurs in the isotropic phase of the LCE, and to the best of our knowledge, no studies

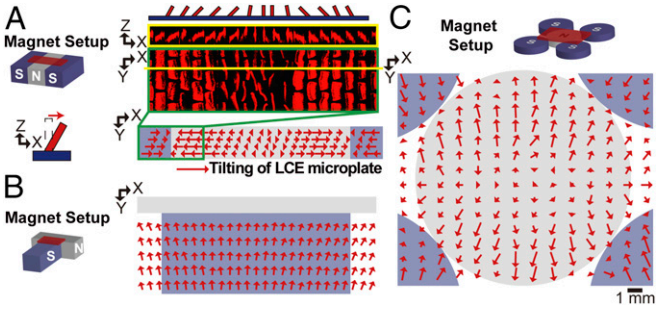

Fig. 4. Fabrication of arrays of LCE microstructures. (*A–C*) Two-dimensional spatial distribution of deformation angles of LCE microplate arrays polymerized in the presence of magnetic fields with (*A*) twofold, (*B*) T-shape, or (*C*) fourfold symmetry. In the schematics of the magnet setup, red blocks represent the position of the LCE microstructure array, and gray and blue blocks show the relative positions of N and S poles of the magnets, respectively. *A*, *Right* shows (*Top* to *Bottom*) a schematic illustration of the deformed array, the corresponding side- and top-view fluorescent confocal micrographs, and a representation of the deformations experienced by each member of the array. Each of the red arrows in *A* and *B* denotes the vector connecting the centers of the top surface of an LCE microplate in its undeformed and deformed states at the corresponding position (shown in *A*, *Inset*), thus indicating the direction and magnitude of tilting of the LCE microplates; in *C*, the arrows represent the average deformation of eight neighboring microplates (see *SI Appendix*, Fig. S10 for original fluorescence confocal micrographs). The gray and purple background denotes the N and S of the magnetic field, respectively.

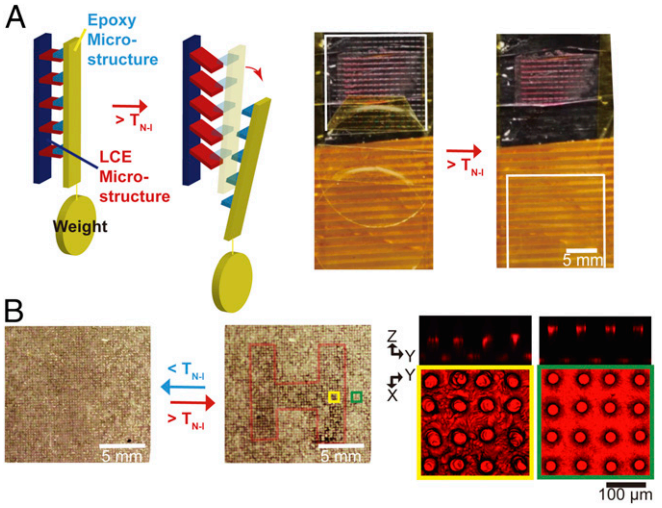

Fig. 5. Potential applications of arrays of LCE microstructures. (*A*) Schematic (*Left*) and experimental realization (*Right*) of a dynamic adhesion system based on cooperative movements of LCE microplates. The white boxes in the photographs indicate the position of the microstructured epoxy cargo (see Movie S4 and *SI Appendix* for more details). (*B*) An information storage system consisting of a stepwise write-in polymerization and a thermally induced readout. (*B*, *Left*) The optical appearance of the microstructure array in the undeformed and deformed states. The region H outside the red boundary was polymerized in the first step, using a mask without a magnetic field; the region inside H was polymerized in the second step upon the removal of the mask in the presence of a magnetic field. (*B*, *Right*) Confocal fluorescence micrographs of the yellow and green regions of the H pattern, showing different deformation modes of the structures polymerized in the first and second steps. Confocal fluorescence micrographs show different deformation behaviors in the regions polymerized at each step.

have reported light-activated deformation of LCE in its isotropic phase. We hypothesize that such an optical responsiveness may be attributed to the combination of (*i*) dynamic structural equilibrium of the internal polymer network induced by the *trans–cis* isomerization of azobenzene cross-linking junctions (Fig. 6*D*); (*ii*) the dynamic thickness of the bimorph induced by the change in transparency of the micropillar at high temperature; and (*iii*) the presence of the surface-anchored mesogens, which unlike the isotropic bulk phase remain partially aligned and whose order is further disrupted by the *trans–cis* isomerization of azobenzene. These results unmask principles by which orthogonal external stimuli can be coupled with deformation modes (i.e., predetermined and self-regulated) to permit the design of multiresponsive actuatable microstructures.

The demonstrated ability of the micropillars to follow the dynamic light source (see *SI Appendix* for details) facilitates progress in the emergent area of self-regulated materials. We envision sensor arrays that combine the notion of each antenna having its own prescribed information (as discussed in Figs. 4 and 5) and controllable response to multiple stimuli (as in Fig. 6 *D* and *E*) to achieve a range of self-regulated responses. This can give rise to multilevel encryption, information processing, autonomous source-following radios, antennae, solar panels, sensors, and unique optical systems for delivering daylight into buildings, all of which hold enormous potential for improving energy efficiency and signal self-optimization. Particularly intriguing is the possibility to employ different sections of the arrays with various ranges of bending angles (Fig. 6*E*) for more efficient light harvesting under different environmental conditions.

We conclude that by applying patterned magnetic fields during the LCE polymerization process, we can encode any desired uniaxial orientation of mesogens in the resulting 3D microstructures. This information can then be read out upon heating in the form of unique, often mechanically unfavored, programmed deformations, including structure elongation and contraction, in- and out-of-plane tilting, and twisting with controlled handedness. These structural reconfigurations are modeled and experimentally demonstrated for exemplary LCE microstructures such as plates, pillars, and honeycomb 3D shapes. Extending this approach to arrays of microstructures synthesized in patterned magnetic fields, we demonstrated cooperative motions of hierarchical microstructure assemblies with pixels of encrypted, area-specific molecular alignments in each member of the array. Such assemblies create opportunities for potential applications in controlled adhesion and information encryption. By further incorporating light-responsive moieties into LCEs, we realized multiresponsive structures that switch their deformation mode between predetermined and self-regulated by the selective application of orthogonal external stimuli; these materials provide the basis for smart energy-harvesting systems. Shear-induced LCE fabrication, such as filamentous 3D printing performed in the presence of a magnetic field, will offer opportunities in creating complex core-shell 3D structures with

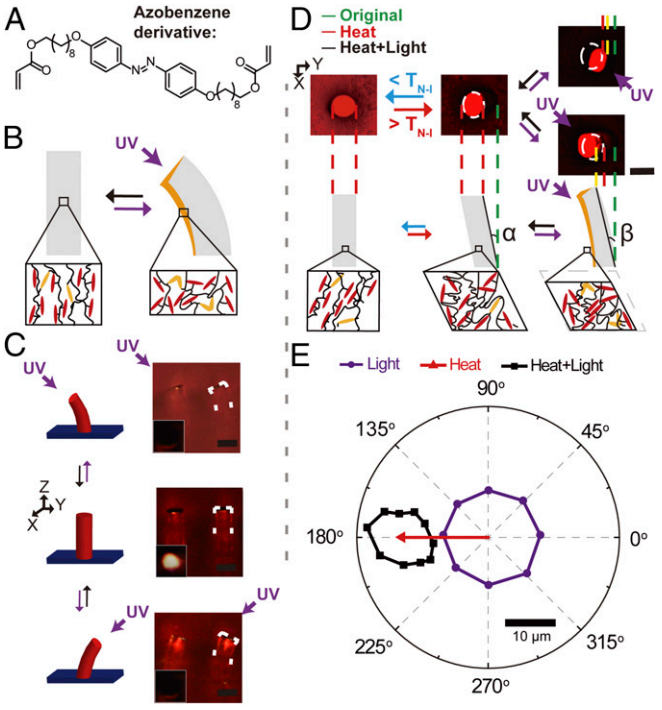

Fig. 6. Light-responsive LCE microactuators. (*A*) Molecular structure of the azobenzene dopant. (*B*) Schematic illustration of the light-responsive LCE microstructure deformation. (*C*) Schematics (*Left*) and corresponding optical micrographs (*Right*) showing self-regulation of LCE micropillars toward the position of the light source. *Insets* show the optical reflection of the silver-coated LCE micropillars (see Movie S7 and *SI Appendix* for more details). Purple arrows represent the direction of the incident UV light. White dashed outlines show the position of the micropillar. (*D*) Fluorescence confocal micrographs (*Top*) and the corresponding schematic illustrations (*Bottom*) of a dual-responsive LCE micropillar. White dashed outlines denote the tip position of the micropillar upon heating above its T_{N-I}. Green, red, and yellow vertical dashed lines show the edge position of the micropillar tip in the original state, heated above T_{N-I}, and exposed to both heating and UV light, respectively. α and β denote the heat-responsive tilting angle and heat–light dual-responsive bending angle of the micropillar. Depending on the direction of the light-exposed wall, $\beta > \alpha$ when light is shone from the direction of the heat-induced tilt (*Bottom Right* confocal micrograph), and $\beta < \alpha$ when shone from the opposite side (*Top Right* confocal micrograph). (*E*) Quantitative characterization of the tip movements of a dual-responsive LCE micropillar subjected to heat, light, and a combination of heat and light.

unique deformation types arising from the superposition of mesogens aligned by the mechanical force and magnetic field. We envision that by combinatorial control over features of the magnetic field, such as strength and direction; mechanical properties of microstructures, including cross-linking density and anisotropy; and other chemically encoded stimuli responsiveness, even more possibilities of deformations and applications can be achieved. The general principles underlying our design can be adapted to a wide range of techniques beyond molding to fabricate classes of materials, such as assemblies of monodisperse adaptive colloidal particles (44) prepared by microfluidics in variable magnetic fields, functional patterned surfaces (45) with dynamic topography achieved by pixelated 3D printing in a magnetic field, mechano-responsive catalysts (46), orthogonal and programmable cargo release (47), and supramolecular materials (48) for multi-responsive soft robots.

Materials and Methods

The LC monomer 4″-acryloyloxybutyl 2,5-di(4′-butyloxybenzoyloxy) benzoate was synthesized following the route described by Thomsen et al. (16). To synthesize thermal-responsive microstructured LCE, the obtained LC monomer was mixed with cross-linker 1,6-hexanediol diacrylate (5% wt/wt based on LC monomer) and photo-initiator 2-hydroxy-2-methylpropiophenone (2% wt/wt based on LC monomer) before polymerization. The reactive mixture was placed into a polydimethylsiloxane (PDMS) mold and covered with a glass substrate. The sample was then placed in a magnetic field (*SI Appendix*, Fig. S5), heated to 90 °C (isotropic phase), cooled down to 60 °C at a rate of 1 °C/min, and exposed to UV (Dymax Model 2000 Flood UV Curing System, light intensity of ∼18 mW/cm^2) in a nitrogen atmosphere to initiate polymerization. After 1 h of polymerization, the sample was cooled down to room temperature, and the PDMS mold was carefully peeled off to get the LCE microstructures. To synthesize photo-responsive LCE micropillars, 4,4′-bis (6-acryloyloxyhexyloxy) azobenzene (7.5% wt/wt based on LC monomer) was added into the reactive mixture described previously; the photoinitiator was changed to bis(2,4,6-trimethylbenzoyl)-phenylphosphineoxide (2% wt/wt based on LC monomer). The sample was placed in a magnetic field, heated to 75 °C, cooled down to 45 °C at a rate of 1 °C/min, and exposed to UV for 1 h with an optical filter that blocks the light with wavelength shorter than 400 nm. The resulting LCE microstructures were actuated by either a heat treatment or exposure to light. Details of sample characterization are in *SI Appendix*.

ACKNOWLEDGMENTS. This material is based upon work supported by the Department of Energy under Award DE-SC0005247 (polymer design and characterization) and by the Department of Defense, Army Research Office under Award W911NF-17-1-0351 (self-regulated optical devices).

1. Vukusic P, Sambles JR, Lawrence CR, Wootton RJ (2001) Structural colour. Now you see it–Now you don't. *Nature* 410:36.
2. Xia F, Jiang L (2008) Bio-inspired, smart, multiscale interfacial materials. *Adv Mater* 20: 2842–2858.
3. Autumn K, et al. (2000) Adhesive force of a single gecko foot-hair. *Nature* 405: 681–685.
4. Tian Y, et al. (2006) Adhesion and friction in gecko toe attachment and detachment. *Proc Natl Acad Sci USA* 103:19320–19325.
5. Erb RM, Sander JS, Grisch R, Studart AR (2013) Self-shaping composites with programmable bioinspired microstructures. *Nat Commun* 4:1712.
6. Capadona JR, Shanmuganathan K, Tyler DJ, Rowan SJ, Weder C (2008) Stimuli-responsive polymer nanocomposites inspired by the sea cucumber dermis. *Science* 319:1370–1374.
7. Schaffner M, et al. (2018) 3D printing of robotic soft actuators with programmable bioinspired architectures. *Nat Commun* 9:878.
8. Le Ferrand H, Bouville F, Niebel TP, Studart AR (2015) Magnetically assisted slip casting of bioinspired heterogeneous composites. *Nat Mater* 14:1172–1179.
9. Kim YS, et al. (2015) Thermoresponsive actuation enabled by permittivity switching in an electrostatically anisotropic hydrogel. *Nat Mater* 14:1002–1007.
10. Zarzar LD, Aizenberg J (2014) Stimuli-responsive chemomechanical actuation: A hybrid materials approach. *Acc Chem Res* 47:530–539.
11. Jeon SJ, Hauser AW, Hayward RC (2017) Shape-morphing materials from stimuli-responsive hydrogel hybrids. *Acc Chem Res* 50:161–169.
12. Fratzl P, Barth FG (2009) Biomaterial systems for mechanosensing and actuation. *Nature* 462:442–448.
13. Terentjev EM, Warner M (2003) *Liquid Crystal Elastomers* (Oxford Univ Press, Oxford).
14. Ohm C, Brehmer M, Zentel R (2010) Liquid crystalline elastomers as actuators and sensors. *Adv Mater* 22:3366–3387.
15. White TJ, Broer DJ (2015) Programmable and adaptive mechanics with liquid crystal polymer networks and elastomers. *Nat Mater* 14:1087–1098.
16. Thomsen DL, et al. (2001) Liquid crystal elastomers with mechanical properties of a muscle. *Macromolecules* 34:5868–5875.
17. Buguin A, Li MH, Silberzan P, Ladoux B, Keller P (2006) Micro-actuators: When artificial muscles made of nematic liquid crystal elastomers meet soft lithography. *J Am Chem Soc* 128:1088–1089.
18. Cui J, et al. (2012) Bioinspired actuated adhesive patterns of liquid crystalline elastomers. *Adv Mater* 24:4601–4604.
19. Liu X, et al. (2015) Reversible and rapid laser actuation of liquid crystalline elastomer micropillars with inclusion of gold nanoparticles. *Adv Funct Mater* 25:3022–3032.
20. Wu ZL, et al. (2013) Microstructured nematic liquid crystalline elastomer surfaces with switchable wetting properties. *Adv Funct Mater* 23:3070–3076.
21. Torras N, Zinoviev KE, Esteve J, Sánchez-Ferrer A (2013) Liquid-crystalline elastomer micropillar array for haptic actuation. *J Mater Chem C Mater Opt Electron Devices* 1: 5183–5190.
22. Shahsavan H, Salili SM, Jákli A, Zhao B (2017) Thermally active liquid crystal network gripper mimicking the self-peeling of gecko toe pads. *Adv Mater* 29:1604021.
23. Ware TH, McConney ME, Wie JJ, Tondiglia VP, White TJ (2015) Actuating materials. Voxelated liquid crystal elastomers. *Science* 347:982–984.
24. Xia Y, Cedillo-Servin G, Kamien RD, Yang S (2016) Guided folding of nematic liquid crystal elastomer sheets into 3D via patterned 1D microchannels. *Adv Mater* 28: 9637–9643.
25. Kotikian A, Truby RL, Boley JW, White TJ, Lewis JA (2018) 3D printing of liquid crystal elastomeric actuators with spatially programed nematic order. *Adv Mater* 30:1706164.
26. Yu Y, Nakano M, Ikeda T (2003) Photomechanics: Directed bending of a polymer film by light. *Nature* 425:145.
27. Camacho-Lopez M, Finkelmann H, Palffy-Muhoray P, Shelley M (2004) Fast liquid-crystal elastomer swims into the dark. *Nat Mater* 3:307–310.
28. Ahir SV, Terentjev EM (2005) Photomechanical actuation in polymer-nanotube composites. *Nat Mater* 4:491–495.
29. van Oosten CL, Bastiaansen CWM, Broer DJ (2009) Printed artificial cilia from liquid-crystal network actuators modularly driven by light. *Nat Mater* 8:677–682.
30. Gelebart AH, et al. (2017) Making waves in a photoactive polymer film. *Nature* 546: 632–636.
31. Palagi S, et al. (2016) Structured light enables biomimetic swimming and versatile locomotion of photoresponsive soft microrobots. *Nat Mater* 15:647–653.
32. de Haan LT, Verjans JMN, Broer DJ, Bastiaansen CWM, Schenning APHJ (2014) Humidity-responsive liquid crystalline polymer actuators with an asymmetry in the molecular trigger that bend, fold, and curl. *J Am Chem Soc* 136:10585–10588.
33. Liu D, Broer DJ (2014) Self-assembled dynamic 3D fingerprints in liquid-crystal coatings towards controllable friction and adhesion. *Angew Chem Int Ed Engl* 53: 4542–4546.
34. McBride MK, et al. (2017) Photoinduced plasticity in cross-linked liquid crystalline networks. *Adv Mater* 29:1606509.
35. Gelebart AH, McBride M, Schenning APHJ, Bowman CN, Broer DJ (2016) Photo-responsive fiber array: Toward mimicking the collective motion of cilia for transport applications. *Adv Funct Mater* 26:5322–5327.
36. Moore JS, Stupp SI (1988) Synthesis of a chemically ordered liquid crystal polymer. *Macromolecules* 21:1217–1221.
37. Mbanga BL, Ye F, Selinger JV, Selinger RLB (2010) Modeling elastic instabilities in nematic elastomers. *Phys Rev E Stat Nonlin Soft Matter Phys* 82:051701.
38. Sawa Y, et al. (2013) Shape and chirality transitions in off-axis twist nematic elastomer ribbons. *Phys Rev E Stat Nonlin Soft Matter Phys* 88:022502.
39. Kuksenok O, Yashin VV, Balazs AC (2008) Three-dimensional model for chemoresponsive polymer gels undergoing the Belousov-Zhabotinsky reaction. *Phys Rev E Stat Nonlin Soft Matter Phys* 78:041406.
40. Horgan CO (2015) The remarkable Gent constitutive model for hyperelastic materials. *Int J Non-linear Mech* 68:9–16.
41. Horgan CO, Saccomandi G (2002) A molecular-statistical basis for the Gent constitutive model of rubber elasticity. *J Elast* 68:167–176.
42. Miller DS, Wang X, Abbott NL (2014) Design of functional materials based on liquid crystalline droplets. *Chem Mater* 26:496–506.
43. Sawa Y, et al. (2011) Shape selection of twist-nematic-elastomer ribbons. *Proc Natl Acad Sci USA* 108:6364–6368.
44. Wang X, et al. (2016) Synthesis of optically complex, porous, and anisometric polymeric microparticles by templating from liquid crystalline droplets. *Adv Funct Mater* 26:7343–7351.
45. Sakamoto T, Nishimura Y, Nishimura T, Kato T (2011) Photoimaging of self-organized $CaCO_3$/polymer hybrid films by formation of regular relief and flat surface morphologies. *Angew Chem Int Ed Engl* 50:5856–5859.
46. Kean ZS, et al. (2014) Photomechanical actuation of ligand geometry in enantioselective catalysis. *Angew Chem Int Ed Engl* 53:14508–14511.
47. Xu W, Ledin PA, Iatridi Z, Tsitsilianis C, Tsukruk VV (2016) Multicompartmental microcapsules with orthogonal programmable two-way sequencing of hydrophobic and hydrophilic cargo release. *Angew Chem Int Ed Engl* 55:4908–4913.
48. Rybtchinski B (2011) Adaptive supramolecular nanomaterials based on strong noncovalent interactions. *ACS Nano* 5:6791–6818.